Structures and physical properties of R_2TX_3 compounds*

Pan Zhi-Yan(潘志艳), Cao Chong-De(曹崇德)†, Bai Xiao-Jun(白晓军),
Song Rui-Bo(宋瑞波), Zheng Jian-Bang(郑建邦), and Duan Li-Bing(段利兵)

Key Laboratory of Space Applied Physics and Chemistry of Ministry of Education, Xi'an 710072, *China*

(Received 3 July 2012; revised manuscript received 6 December 2012)

Rare-earth compounds have been an attractive subject based on the unique electronic structures of the rare-earth elements. Novel ternary intermetallic compounds R_2TX_3 (R = rare-earth element or U, T = transition-metal element, X = Si, Ge, Ga, In) are a significant branch of this research field due to their complex and intriguing physical properties, such as magnetic order at low temperature, spin-glass behavior, Kondo effect, heavy fermion behavior, and so on. The unique physical properties of R_2TX_3 compounds are related to distinctive electronic structures, crystal structures, micro-interaction, and external environment. Most R_2TX_3 compounds crystallize in AlB_2-type or derived AlB_2-type structures and exhibit many similar properties. This paper gives a concise review of the structures and physical properties of these compounds. Spin glass, magnetic susceptibility, resistivity, and specific heat of R_2TX_3 compounds are discussed.

Keywords: R_2TX_3 compounds, structure, physical properties

PACS: 61.50.–f, 75.20.En, 72.80.Ga, 75.30.Gw **DOI:** 10.1088/1674-1056/22/5/056102

1. Introduction

Rare-earth compounds have significant applications in a variety of fields for they can be synthetized into rare-earth luminescent materials, hydrogen-storage materials, superconducting materials, magnetic materials, etc. Hence, more and more rare-earth compounds have been synthetized and investigated, yielding fruitful outcomes, opening up exciting avenues, and also throwing up challenges. The magnetic order and even multiple magnetic order at low temperature, the giant magnetoresistance (GMR) effect, spin-glass behavior, heavy fermion behavior, and magnetocaloric effect (ME) have been constantly revealed in rare earth-transition metal intermetallic compounds in recent years. Recently, R_2TX_3 compounds have been attracting much attention because of their unique properties (especially magnetic behaviors). Most 2:1:3-type compounds are crystallized in an AlB_2-type structure, and some members have superstructures, while others may have their rare-earth ions occupy two different sites. Researchers have been exploring the crystal structures and magnetic structures through neutron diffraction.

In the present paper, we review and discuss the crystallographic structures and typical physical properties of 2:1:3-type rare-earth compounds.

2. Rare-earth elements and rare-earth compounds

Rare-earth elements (REEs) consist of lanthanide series with atomic number ranging from 57 to 71, scandium (atomic number 21), and yttrium (atomic number 39). The electronic configuration of rare-earth elements is $(Xe)4f^{0-14}5d^{0-1}6s^2$ with partially filled 4f electron layers, usually displaying the state of trivalence except for cerium, europium, and yttrium, which often display valence fluctuation in their compounds. Rare-earth elements are characterized by localized 4f electrons, which are shielded by the outer $5s^2$–$5p^6$ electrons,[1,2] and to some extent by 5d–6s electrons. Their orbital magnetic moment is therefore protected from the crystal field, and the phenomenon of quenching of orbital angular momentum (which occurs to 3d magnetics) will not exist. The magnetic moment formed by 4f electrons is the key source of the magnetism of rare-earth elements. It has been found that many rare-earth magnetics exhibit a stronger spontaneous magnetization than common magnetic materials. This separates the rare-earth magnetics into a separate class particularly from the point of view of electron structure, which has stimulated researchers to initiate deep and detailed research on rare earths and rare-earth compounds.

Since Rauchschwalbe *et al.*[3] discovered heavy fermion superconductor compounds $CeCu_2Si_2$, many rare earth-transition metal intermetallic compounds have been widely investigated. For instance, Kondo lattice $CePt_2Si_2$,[4–8] superconductor $CePd_2Si_2$,[9–11] complex magnetism Eu_2PdSi_3,[12–14] ferromagnetic order and weak spin-glass Pr_2CuSi_3,[15,16] etc. In rare-earth compounds, 4f electrons interact with conduction electrons, and 4f electrons themselves also interact with each other, which manifests in

*Project supported by the National Natural Science Foundation of China (Grant No. 51171152), the Doctoral Fund of Ministry of Education of China (Grant No. 20126102110048), the Research Fund of State Key Laboratory of Solidification of China (Grant No. SKLSP201202), the Open Research Fund of State Key Laboratory of Electronic Thin Films and Integrated Devices (UESTC) of China (Grant No. KFJJ201103), the NPU Foundation for Fundamental Research of China (Grant No. JC201268), and the Natural Science Basic Research Plan in Shaanxi Province, China (Grant No. 2012JC2-02).

†Corresponding author. E-mail: caocd@nwpu.edu.cn

© 2013 Chinese Physical Society and IOP Publishing Ltd

competition between Kondo effect and RKKY interaction.[17] However, the Kondo effect is inclined to reduce magnetic moment, while the Ruderman–Kittel–Kassuya–Yosida (RKKY) interaction tends to stabilize it. The compounds susceptible to these effects may present resistance anomaly, high specific heat coefficient γ, high magnetic susceptibility χ, or high thermoelectric potential S.

3. 2:1:3-type rare earth-transition metal intermetallic compounds

The system of R_2TX_3 has become the subject of intensive studies. Inside the system, there are respective families categorized as R_2NiGe_3,[18] R_2PdSi_3,[19–24] R_2RhSi_3,[25,26] R_2AgIn_3,[27,28] R_2CuIn_3,[29–31] etc. Each family usually presents almost similar properties. For example, R_2RhSi_3 and R_2PdSi_3 (R = Ce, Gd, Tb, Dy, Ho, Er) compounds order antiferromagnetically, while the Nd compound orders ferromagnetically. Most R_2AgIn_3 compounds do not show long-range magnetic order except Tb_2AgIn_3[32] and Tm_2AgIn_3.[33] There are similar magnetic features in the Tb_2AgIn_3 and Tm_2AgIn_3 compounds. This may be associated with the fact that in the ground state the Tb and Tm ions share identical values of L and S (L=5 and S=1). All the R_2CuIn_3 (R=Nd, Dy, Ho) compounds order antiferromagnetically. In addition, compounds U_2TX_3 with T= Pd, Pt, Au, Ir, Rh are found to show spin-glass or cluster glass behavior below their respective spin freezing temperature. Owing to the existence of rare-earth elements, the behavior of R_2TX_3 is consistent, to some degree with the compounds or alloy composed of rare-earth and other elements. In these compounds, the Kondo effect often countersigns itself as the anomaly in electrical resistivity and specific heat, which may also be responsible for the effective mass enhancement. The major parameter to characterize the magnetic properties is magnetic susceptibility χ at different temperatures. It always presents the basic information about the compounds. Generally, we find anomalies characterized by the occurrence of peaks at low temperature, indicating magnetic transition. There is even more than one magnetic transition in some compounds. Take Tb_2CuGe_3[34] as an example, there are three magnetic transitions, all of which are of antiferromagnetic type, namely 20, 13, and 8 K. At these temperatures, Tb_2CuGe_3 has different Fermi surfaces arising from changes in the magnetic structures. Nowadays, a large number of R_2TX_3 compounds have been synthetized. Among them, La_2TX_3 and Lu_2TX_3 are generally regarded as the isomorphic nonmagnetic counterpart, providing reference to other R_2TX_3 compounds because their electronic allocations are characterized by $4f^05d^16s^2$ for La and $4f^{14}5d^16s^2$ for Lu, and hence display no magnetism. However, not all their references are available because some of them form multiphases. Although quite a few single crystals have been synthesized, there are still challenges to grow single crystals with high quality for some R_2TX_3. Thus, polycrystals will still occupy an important position in the research field of R_2TX_3 compounds. Consequently, both fundamental and applied research in this field are of great significance.

4. Structure of 2:1:3-type rare-earth ternary compounds

In 1967, Raman[35] firstly explored R_2CuSi_3 (R=La, Ce, Er), R_2Cu_3Si (R=Ce, Nd, Gd, Y, Er), and La_2FeSi_3, La_2NiSi_3, Ce_2NiSi_3 compounds. These silicides crystallize in an AlB_2-type structure(β-$ThSi_2$-type structure), which belongs to space group $P6/mmm$ with lattice parameter $c/a \approx 1$, except that Er_2CuSi_3 crystallizes in α-$ThSi_2$-type structure and space group of $I4_1/amd$ (maybe originating from the change of valence electron concentration[36]). In 1984, Chevalier and his coworkers[37] prepared R_2RhSi_3 (R = Y, La, Ce, Nd, Sm, Gd, Tb, Dy, Ho, Er), and found that these kinds of compounds appear in derived AlB_2-type superstructures and their lattice parameters a and c are about twice those of their disilicides RSi_2. In 1990, researchers prepared a series of R_2PdSi_3 compounds in order to search bizarre materials, and what attracted the subsequent researchers was that R_2PdSi_3 compounds have considerable structural similarity with rare-earth disilicides and R_2RhSi_3. In 1996, Hwang *et al.*[38] synthetized polycrystalline Ce_2CuSi_3 and La_2CuSi_3, and confirmed the AlB_2-type structure, which Raman suggested previously. In 1999, Szytuła *et al.*[39] studied R_2PdSi_3 (R=Ce, Nd, Tb, Er) and found that all these R_2PdSi_3 compounds formed an AlB_2-type structure. Later, Tang *et al.*[40] conducted a systematic study on heavy rare-earth compounds R_2PdSi_3 (R=Gd, Tb, Dy, Ho, Er, Tm), which revealed the existence of a crystallographic superstructure via X-ray and neutron diffraction. The unit cell parameter a is found to be about 8 Å. Initial neutron diffraction experiments on powder samples by Szytuła *et al.* indicated, however, a primitive AlB_2-type structure with randomly occupied 2d sites, which is the currently accepted crystal structure. The lattice constants (see Table 1) are about 4 Å for both a and c throughout the series. It is not clear yet that which model is the source of the superstructure, and the inconformity between the X-ray and neutron diffraction indicates the structural complexity of R_2PdSi_3. In recent years, researchers successively synthetized a series of R_2AgIn_3[27] compounds, which crystallize in a $CaIn_2$-type structure, and belong to space group $P6_3/mmc$ with lattice parameter $c/a = 0.792$ ($Z = 2$). The $CaIn_2$-type structure is the deformation variance of the AlB_2-type structure reported in the Refs. [41] and [42]. In the meantime, the series of U_2TX_3 compounds consisting of actinide element U, which have a unique 5f electronic structure, have also become a hot research topic. In 1993, Pöttgen[43] synthetized 11 uranium silicides U_2TSi_3 (T=Fe, Co, Ni, Cu,

Ru, Rh, Pd, Os, Ir, Pt, Au). Most of these compounds crystallize in an AlB_2-type structure, with partly or completely crystallographic disorder of T and Si within B positions. Besides, U_2CuSi_3[44] forms a tetragonal α-$ThSi_2$ structure, and U_2FeSi_3, U_2RuSi_3, and U_2OsSi_3 crystallize in a U_2RuSi_3-type structure with complete order in B site. In 1996, Tran[45] reported the synthesis of the series of U_2TGa_3 (T=Ru, Rh, Ir, Pd, Au, Pt), and found that they crystallize in $CeCu_2$ type, which belongs to space group *Imma*. To sum up, the crystal structures of most R_2TX_3 are identified to be in AlB_2 type or derived AlB_2 type, which consist of R–R magnetic layer and T–X layers alternating along the c axis, and possible crystallographic disorder within T–X positions. Figure 1(a) shows the unit cell of the AlB_2 structure. The unit cell of AlB_2 contains only three atoms. It corresponds to a simple hexagonal unit cell of aluminum atoms (Wyckoff site 1a) with the two boron atoms occupying the trigonal prismatic sites (Wyckoff site 2d). For R_2TX_3 compounds, it is possible to obtain AlB_2-related structures, where the R atoms occupy the aluminum positions, while the T and X atoms form the hexagons (boron positions). This distribution can be expected to cause some anomalous physical properties, which will be described below. Figure 1(b) presents the projection of typical AlB_2 structure (U_2TSi_3,[46] T=Ru, Rh, Pd) onto the hexagonal plane, showing different degrees of order. We performed the XRD measurement of Tb_2NiSi_3 and obtained the typical AlB_2 structure,

Table 1. Crystallographic parameters and crystal types of several R_2TX_3 compounds.

Compound	a/Å	b/Å	c/Å	Structure type
Ce_2CuGe_3[47]	7.262	4.591	4.231	orthorhombic
La_2CuGe_3[47]	7.260	4.608	4.465	orthorhombic
Yb_2AuGe_3[48]	805124(17)	14.730(2)	8.4995(17)	orthorhombic
Tb_2CuGe_3[34]	4.062		4.077	AlB_2-type
U_2AuGa_3[49]	4.435	7.079	7.799	orthorhombic $CeCu_2$-type
Ce_2CuSi_3[38]	4.059(1)		4.294(4)	AlB_2-type
Pr_2CuSi_3[16]	4.052		4.255	AlB_2-type
La_2CuSi_3[38]	4.084		4.395	AlB_2-type
Ce_2RhSi_3[50]	8.2310(3)		8.4391(3)	Er_2RhSi_3-type
Nd_2RhSi_3[51]	8.186		8.272	Er_2RhSi_3-type
Gd_2RhSi_3[51]	8.112		7.976	Er_2RhSi_3-type
Tb_2RhSi_3[51]	8.110		7.860	Er_2RhSi_3-type
Dy_2RhSi_3[51]	8.097		7.823	Er_2RhSi_3-type
Ho_2RhSi_3[51]	8.072		7.771	Er_2RhSi_3-type
Y_2RhSi_3[51]	8.086		7.829	Er_2RhSi_3-type
La_2RhSi_3[51]	8.233		8.594	Er_2RhSi_3-type
Er_2RhSi_3[52]	8.1130		7.7556	ordered variant of AlB_2-type
Lu_2CoGa_3[52]	8.659		6.823	ordered variant of AlB_2-type
Ce_2IrSi_3[53]	8.2120 (7)		4.2374(4)	U_2RuSi_3-type
Ce_2CoSi_3[53,54]	8.104(1)		4.197(1)	U_2RuSi_3-type
U_2FeSi_3[55]	8.003		3.854	U_2RuSi_3-type
U_2RuSi_3[55]	8.145		3.8496	ordered variant of AlB_2-type
Ce_2FeSi_3[54]	4.065		4.191	AlB_2-type
Ce_2NiSi_3[56]	4.0485(1)		4.2877(1)	AlB_2-type
La_2NiSi_3[56]	4.0711(4)		4.3737(6)	AlB_2-type
Dy_2PdSi_3[57]	4.062		4.031	AlB_2-type
Eu_2CuSi_3[58]	4.095		4.488	AlB_2-type
Nd_2PtSi_3[59]	4.0927		4.2582	AlB_2-type
Tb_2CuIn_3[60]	4.702(1)		3.682(1)	AlB_2-type
U_2CuGa_3[61]	4.348(1)		3.605(1)	AlB_2-type
U_2IrSi_3[55]	4.090		3.954	AlB_2-type
U_2PdSi_3[62]	4.083		3.932	AlB_2-type
U_2PtSi_3[63]	4.073(6)		3.960(3)	AlB_2-type
U_2RhSi_3[46]	4.074		3.881	AlB_2-type
U_2CoSi_3[46]	3.988		3.883	AlB_2-type
U_2NiSi_3[46]	3.979		3.949	AlB_2-type
Tm_2AgIn_3[33]	4.778		7.146	$CaIn_2$-type
Tb_2AgIn_3[32]	4.793(1)		7.322(2)	$CaIn_2$-type
Nd_2AgIn_3[64]	4.8826		7.584	$CaIn_2$-type
Pr_2AgIn_3[65]	4.872(2)		7.594(4)	$CaIn_2$-type
Ce_2PdSi_3[20]	4.1215(13)		4.2723(22)	AlB_2-type
Nd_2PdSi_3[20]	4.1033(16)		4.2039(24)	AlB_2-type
Tb_2PdSi_3[20]	4.0642(15)		4.0502(41)	AlB_2-type
Ho_2PdSi_3[20]	4.0459(7)		3.9977(13)	AlB_2-type
Er_2PdSi_3[20]	4.0427(20)		3.9794(29)	AlB_2-type
Tb_2NiSi_3	3.9672,		4.0429	AlB_2-type

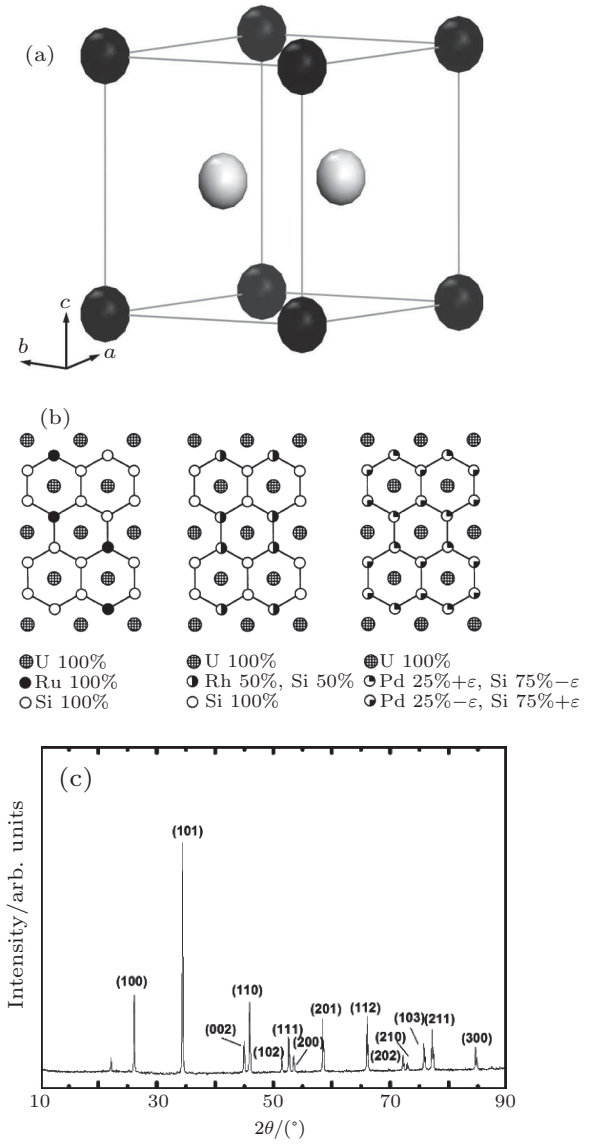


Fig. 1. (a) The unit cell of an AlB_2 structure with Al atoms at the 1a position and B atoms distributed in a plane between the Al atoms. (b) The crystal structure of a typical AlB_2 structure (U_2TSi_3,[46] T=Ru, Rh, Pd) projected onto the hexagonal ab plane. For U_2PdSi_3, the weak tendency to an orthorhombic superstructure of Pd and Si atoms is indicated by $\varepsilon \geqq 0$. (c) X-ray powder diffraction pattern for Tb_2NiSi_3.

as shown in Fig. 1(c). Hitherto, the synthesis and research of rare-earth ternary compounds are developing vigorously. More and more R_2TX_3 compounds are brought into synthesis and structural exploration. Table 1 shows crystallographic parameters and crystal types of several R_2TX_3 compounds. In this table, many compounds are actually derived (in view of the ratio change in the crystal parameters a and c, or the degree of order of atomic sites) AlB_2-type, but share the same AlB_2-type steric configuration, and thus are calibrated to be AlB_2 type. Besides, we need to explain the reason why Er_2RhSi_3 ($2a$, $2c$), Lu_2CoGa_3 ($2a$, $2c$), and U_2RuSi_3 ($2a$, c) are all ordered variances of the AlB_2-type structure. The Lu_2CoGa_3 structure is a distorted AlB_2-type structure, where the trigonal Lu_6 prisms centered by cobalt atoms share triangular faces in infinite columns. The distortions in Er_2RhSi_3 are of a lesser magnitude than those observed in Lu_2CoGa_3. Ce_2CuGe_3, La_2CuGe_3, and Yb_2AuGe_3[48] form the orthorhombic (space group: *Fmmm*) ordered superstructure of AlB_2 type. Based on various structures, R_2TX_3 shows diversity of magnetic ground states, which makes it possible for them to behave differently from each other from the point of view of physical properties.

5. Magnetic order behavior

It has been confirmed that magnetic order originates from electronic exchange interaction. For rare-earth compounds, the unique 4f electrons determine that the interaction between ions is RKKY indirect exchange interaction, instead of Heisenberg coupling. The typical behaviors of magnetic order are ferromagnetic order (FM) and antiferromagnetic order (AFM). The type of magnetic order can be determined by interatomic distance and the radius of electronic orbit. Almost all R_2TX_3 compounds display FM or AFM at low temperatures, and we can judge this behavior by magnetic susceptibility. At Curie temperature, the thermal energy of electronic spins can counterbalance the magnetic field energy of electrons imposed by a molecular field. Thus, the material will lose magnetism. According to Curie–Weiss law

$$\chi = C_0/(T - \Theta_p), \tag{1}$$

where C_0 is the Curie constant, T is temperature, the sign of Θ_p will determine the type of magnetic order, which can be deduced from the linear part of the magnetic susceptibility curve, the negative for AFM and positive FM. The effective moment μ_{eff} can be derived from

$$C_0 = N\mu_{eff}^2/3k_B, \tag{2}$$

while in the case of free ions,

$$\mu_{eff} = \mu_B g\sqrt{J(J+1)}, \tag{3}$$

where N is the Avogadro constant, k_B is Boltzmann's constant, μ_B is the Bohr magneton, g is the Lande factor, and J is the total angular momentum quantum number. The effective moment obtained from linear region cannot be in complete agreement with that of free ions due to different reasons. For example, μ_{eff} for Tb_2CuIn_3[60] is $10.3\mu_B$ per Tb ion, while $9.72\mu_B$ for free ion, due to conduction electron polarization. The μ_{eff} of Tb_2AgIn_3[32] is $5.1\mu_B$ per Tb ion, much smaller than $9.72\mu_B$ for free ion. It is the crystal electric field and frustration effects caused by the statistical distribution of Ag and In atoms that prevent the formation of the full magnetic moment on the Tb ions.[32] Table 2 shows the effective magnetic moments and magnetic moments for free ions of some R_2TX_3 compounds. Remarkably, the magnetic behaviors are obviously different in the zero field cooling (ZFC) and field cooling (FC) states for most R_2TX_3 compounds. When temperature is

lowered to a certain point, the divergence of magnetic susceptibility occurs between the ZFC and FC curve. Owing to different conditions of applying magnetic field, when the cooling process is finished, random-frozen magnetic ion moments are formed in the sample experiencing the ZFC process, while the FC condition facilitates the formation of magnetic moments towards the direction induced by the external magnetic field. After increasing the temperature, both tend to rotate towards an external field, but the initial state before increasing temperature and the competitive effect between the thermal energy and magnetic energy will eventually result in the divergence under different conditions. This phenomenon may originate from spin-glass behavior (such as Ce_2CuGe_3[47]), strong magnetic anisotropy (such as Eu_2CuSi_3[58]), grain-boundary pinning effect or domain-wall pinning effect, and superparamagnetism. Figure 2 shows the difference between χ_{FC} and χ_{ZFC} for compounds Dy_2AuSi_3 and Nd_2PtSi_3. The irreversibility in the two compounds results respectively from FM cluster-glass behavior and the formation of ferromagnetic order. For the Dy_2AuSi_3 compound, the irreversibility temperature T_{ir} is much larger than the peak temperature T_m in χ_{ZFC} curve. This phenomenon is different from that observed for standard SG materials, and can be considered as a characteristic feature for a ferromagnet with high magnetic anisotropy or a short-range FM order (FM cluster) system. While for the Nd_2PtSi_3 compound, the deviation between χ_{FC} and χ_{ZFC} starts at T_c ($T_{ir} = T_c$) at very low applied fields. This observation means that the irreversible magnetism results from the formation of ferromagnetic state.

The form of magnetic order is various. Hwang *et al.*[38] pointed out that polycrystalline Ce_2CuSi_3 shows an antiferromagnetic order at 2.1 K in a field of 50 Oe, whereas this ordering peak was smeared in a field of 2000 Oe. This anomaly phenomenon implies a conical ferromagnetic helical spin structure. Frontzek *et al.*[66] performed neutron diffraction and AC susceptibility measurement on Tb_2PdSi_3 single crystal, and reported the existence of strong anisotropy. In the c direction, the Curie–Weiss behaviors can be observed only above 150 K, producing AFM coupling. In contrast, the Curie–Weiss behavior appears from right above 23 K in the basal plane, causing FM coupling. In fact, many ferromagnetic compounds exhibit strong magnetocrystalline anisotropy, which results from the competing effects of the crystal electric field (CEF) and the magnetic two-ion interaction. In addition, the deviation from Curie–Weiss law of magnetic susceptibility at low temperature is the result of the combination of the CEF effect, exchange interaction, and Kondo effect. The crystal electric field is referred to as the effect of nearest atoms and ions, and it could be equivalent to a certain potential field. the CEF effect can cause the splitting of the ground state of rare-earth ions, which will further leads to the change of specific heat, electric resistance, and other properties. However, the CEF is a single-ion property and two-ion exchange interactions are needed to mediate order. The crystalline electric field, energy level, and degeneracy-splitting of energy level are strongly dependent on crystal symmetry.

Table 2. Effective magnetic moments and magnetic moments for free ions of R_2TX_3 compounds.

	Compound	μ_{eff}/μ_B	μ_{effR}/μ_B
Ce	Ce_2NiGe_3[67]	2.57	2.54
	Ce_2CuSi_3[38]	1.95	
	Ce_2NiSi_3[56]	2.57	
	Ce_2CuGe_3[47]	2.40	
	Ce_2RhSi_3[51]	2.40	
Tb	Tb_2CuGe_3[34]	10.80	9.72
	Tb_2PdSi_3[68]	9.87	
	Tb_2CuIn_3[60]	10.30	
	Tb_2AgIn_3[32]	5.10	
	Tb_2RhSi_3[51]	9.61	
Dy	Dy_2NiGe_3[18]	10.68	10.63
	Dy_2PdSi_3[57]	10.65	
	Dy_2RhSi_3[51]	10.67	
Pr	Pr_2NiGe_3[18]	3.59	3.58
	Pr_2CuSi_3[16]	3.54	
Nd	Nd_2NiGe_3[18]	3.65	3.62
	Nd_2CuSi_3[15]	3.68	
	Nd_2RhSi_3[51]	3.76	
Gd	Gd_2NiGe_3[18]	8.00	7.94
	Gd_2RhSi_3[51]	7.61	

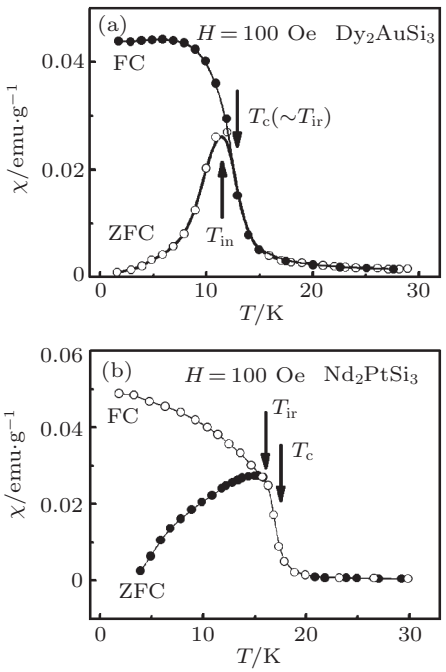


Fig. 2. (a) The divergence between χ_{FC} and χ_{ZFC} for compound Dy_2AuSi_3[69] and Nd_2PtSi_3.[59] The irreversible magnetism is from FM cluster-glass behavior. (b) The formation of ferromagnetic order.

6. Spin-glass behavior of R_2TX_3

A spin glass (SG) is a disordered magnet with frustrated interactions of atomic magnetic moment. It is a common belief that quenched disorder and frustration are the necessary

conditions to form an SG state where ferromagnetic and antiferromagnetic bonds exist paradoxically. In R_2TX_3(exclude U_2TX_3), the statistical distribution of T and X atoms crystallographically produces a varying environment around R ions and causes a variation in RKKY mediated exchange interaction, which will facilitate the formation of spin glass. A host of R_2TX_3 compounds due to distinctive structures display SG behavior. We enumerate them as follows: U_2TSi_3[70] (T= Pd, Pt, Au, Ir, Rh) show SG or cluster glass behavior. In rare-earth compounds, there are typical SG behavior in Ce_2NiGe_3,[67] Pr_2AgIn_3,[65] Ce_2AgIn_3,[71] and Ce_2CuGe_3.[47] Coexistence of SG state with long-range magnetic order exists in Pr_2CuSi_3,[15] Nd_2CuSi_3,[15] Dy_2CuIn_3,[72] and Gd_2CuIn_3.[73] Weak spin glass exists in Nd_2PtSi_3,[59] re-entrant spin-glass Dy_2PdSi_3,[57] and Ce_2CuGe_3.[47] Canonical SG compounds always show the following features.[47,59,61,64,69] (i) The peak position T_f in $\chi_{ZFC}(T)$ curve strongly depends on the external magnetic field. Both peak position T_f and T_{ir} (irreversibility temperature is usually defined as the temperature below which χ_{FC} and χ_{ZFC} curves separate from each other) shift to low temperatures with increasing external magnetic field. (ii) There is pronounced irreversible magnetism below T_{ir} behaving as the divergence between χ_{FC} and χ_{ZFC} curves. (iii) Both the real and the imaginary part of AC magnetic susceptibility form obvious peaks close to T_f whose positions shift towards higher temperatures with increasing frequency. The magnitude of the real component at the maximum decreases, and that of the imaginary component rapidly increases with the increase in frequency. Figure 3 shows real component $\chi'_{ac}(T)$ of the AC susceptibility versus temperature at various frequencies for typical spin-glass behavior. (iv) T_f coincides with T_{ir} for a simple spin glass. (v) Remnant magnetization and magnetic relaxation on macroscopic time scales after changing the applied magnetic field below T_f are also typical signals of spin-glass behavior, as shown in Fig. 4. The different extents of magnetic relaxation are shown for Nd_2AgIn_3,[64] U_2RhSi_3,[46] and Pr_2CuSi_3.[15] The relaxation characteristic can be described as follows:[54]

$$M_{IRM}(t) = M_0(t) - \alpha(t)\ln(t), \tag{4}$$

where IRM denotes the isothermal remnant magnetization, M_0 is the initial zero-field magnetization, and $\alpha(t)$ is the viscosity coefficient. While for nonmagnetic disorder (NMAD) spin glass, there is the exponential term in the expression of $M_{IRM}(t)$:[74]

$$M_{IRM}(t) = M_0 + \alpha ln(t) + \beta exp(-t/\tau), \tag{5}$$

where M_0, α, β, and τ are fitting parameters. (vi) The SG system lacks periodic long-range magnetic order. (vii) $\chi_{FC}(T)$ for a canonical SG tends to be nearly constant below T_f. (viii) The imaginary part of AC magnetic susceptibility will vanish just above T_f, which is expected for a paramagnet. Apart from all the above features, the magnetic entropy of an SG system is much lower than the ordered system empirically and experimentally. There are two typical formulas to describe spin-glass behavior. The initial frequency shift δT_{ac} can be calculated by[15]

$$\delta T_{ac} = \Delta T_{ac}/(T_{ac}\Delta \log w). \tag{6}$$

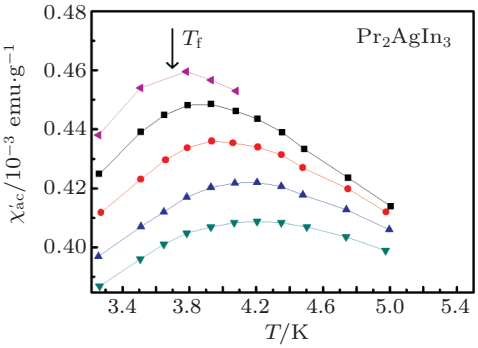


Fig. 3. (color online) Real component $\chi'_{ac}(T)$ of the ac susceptibility of Pr_2AgIn_3 versus temperature at various frequencies of 0.1, 1, 10, 100, and 1000 Hz (from top to bottom).[65]

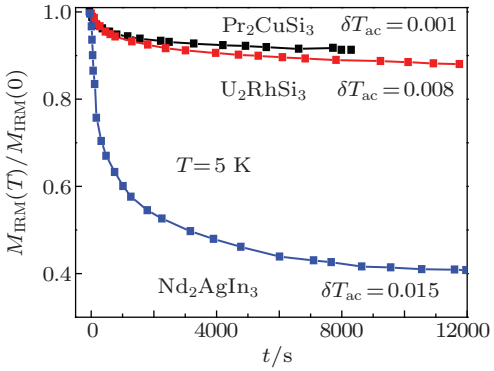


Fig. 4. (color online) Time dependence of the isothermal remnant magnetization $M_{IRM}(t)/M_{IRM}(0)$ for Nd_2AgIn_3,[64] U_2RhSi_3,[46] and Pr_2CuSi_3.[15] The magnitude of δT_{ac} measures the extent of the formation of spin glass.

This formula is usually applied to distinguish an SG material from an SG-like system, where T_{ac} (or T_f) is always defined as the peak temperature of magnetic susceptibility, w represents the frequency, δT_{ac} is about several percent in typical spin-glass system. Figure 5 shows the δT_{ac} values of several R_2TX_3 compounds, indicating the intensity of spin glass. The Vogel and Fulcher empirical equation can also be used to analyze the frequency dependence of AC susceptibility[74]

$$w = w_0 \exp\left(-\frac{E_a}{k_B(T_f - T_0)}\right), \tag{7}$$

where w_0 is the characteristic frequency, E_a the activation energy, T_0 the Vogel–Fulcher temperature, and k_B the Boltzmann constant. For a spin-glass system, the characteristic temperature T_0 is somewhat lower than the Curie temperature.

In fact, most spin-glass behaviors in R_2TX_3 system are not simple ones. As we discussed above, SG arises from frustration. This means that there must be a competition between ferromagnetic and antiferromagnetic interactions. For R_2TX_3 compounds, within one magnetic layer R atoms form triangles of nearest neighbors and no single configuration of the spins is extraordinarily favored by all interactions. Therefore, on account of different degrees of structural disorder of nonmagnetic atoms and different strengths of random frustration of *R*–*R* interactions, it is easy to understand that there exists a wide range from a simple spin glass to a spin glass with ferromagnetic to a long-range magnetic order. In 2008, Li *et al.*[15] explained the phenomenon in terms of magnetic cluster, establishing that the disorder of nonmagnetic atoms could destroy the long-range magnetic correlation and result in the formation of finite-size granules with net magnetic moments (magnetic clusters) which can interact with each other at low temperature. The size of magnetic cluster depends on the degree of randomness and relative strength of magnetic interaction. When *T* and *X* atoms are distributed with complete disorder, the cluster is so small that it forms a simple SG (instead of superparamagnetic behavior due to the fact that the magnetic moments are randomly distributed within every cluster). With the increase in the degree of order, the cluster becomes larger and the properties vary from simple SG to cluster glass. Moreover, Li *et al.* interpreted the NMAD spin-glass behavior of R_2TX_3 commendably. On the other hand, there is another well-known phenomenon, reentrant spin glass, which has been discovered in some R_2TX_3 compounds, such as Dy_2PdSi_3,[57] and U_2RhSi_3.[66] Reentrant spin-glass transition is found near the phase boundary between the SG phase and the ferromagnetic phase. It is a reentry from a magnetic order to a frozen state with magnetic cluster. However, there is not a unanimously perfect theory that can demonstrate the mechanism of reentry. Further research is needed to explain the distinctive phenomenon. Because no long-range magnetic order exists in spin-glass system, the ρ–T curve and C–T curve of this kind of compounds do not show sharp peaks. However, it has been confirmed that the spin-glass magnetism can result in enlargement of specific heat coefficient, as suggested by Gschneidner *et al.*[75]

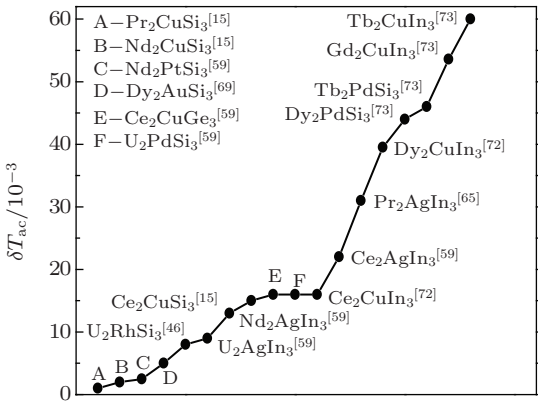


Fig. 5. The δT_{ac} values of several R_2TX_3 compounds. The pattern indicates the intensity of different R_2TX_3 compounds.

7. Electrical resistivity and specific heat of R_2TX_3

During the research of R_2TX_3 compounds, the measurement of resistivity and specific heat is a major method. Some important information is usually obtained by comparing curves of ρ–T, C–T, and χ–T. The occurrence of magnetic order is reflected together on the three curves, characterized by the change of slope or the occurrence of peak. Over the low-T region, the appearance of magnetic-related scattering leads to the change of resistivity, and magnetic oscillation brings about the anomaly of specific heat. Usually, the changes in ρ and C take place consistently near the magnetic phase transition temperature. Even for complex phase, ρ and C can still reflect consistently the magnetic properties. However, for Tb_2CuGe_3, Majumdar *et al.*[34] found there was no significant drop of ρ near the transition at 20 K, which was expected to occur according to C and χ. This indicates that the transition around 20 K is related to the formation of magnetic Brillouin-zone boundary gaps in a way that the drop due to the loss of spin-disorder contribution to ρ is nearly compensated by an increase in ρ.

The resistivity of R_2TX_3can be regarded as the summation of the following contribution:[16]

$$\rho(T) = \rho_{\rm imp} + \rho_{\rm ph}(T) + \rho_{\rm m}(T), \tag{8}$$

where $\rho_{\rm imp}$ is also called residual resistivity, which results from the scattering of impurities and lattice imperfections, $\rho_{\rm ph}(T)$ is the contribution of the electro-phonon interaction, and $\rho_{\rm m}(T)$ is caused by the magnetic scattering. The residual resistivity takes typically smaller values in ferromagnets, while much larger values $\rho_{\rm imp}$ are observed in antiferromagnets. As we mentioned above, the La_2TX_3 compound is characterized by analogous crystal structure with other R_2TX_3 compounds. The lattice contribution is roughly identical for La_2TX_3 and other R_2TX_3 compounds, and thus the resistivity caused by magnetic scattering for R_2TX_3 compounds can be derived as

$$\rho_{\rm m}(T) = \rho(R_2TX_3) - \rho(La_2TX_3). \tag{9}$$

Similarly, the specific heat can be expressed as

$$C = C_{\rm e} + C_{\rm ph} + C_{\rm m}, \tag{10}$$

where $C_{\rm e}$ and $C_{\rm ph}$ are the specific heat resulting from the contribution of electrons and lattice vibration, respectively. The $C_{\rm m}$ represents the magnetic specific heat.

The magnetic part of specific heat[67] reads

$$C_{\rm m}(T) \approx C(R_2TX_3) - C(La_2TX_3). \quad (11)$$

In standard metallic system, the dominating resistance mechanism is electron-phonon scattering, which leads to monotonous decrease in $\rho(T)$ with the decrease in temperature. However, for many rare-earth compounds, electrical resistivity is characterized by Kondo behavior. It is believed that Kondo effect results from the coupling of localized magnetic impurities and itinerant electrons. At low temperatures, apart from residual resistance, the leading mechanism for resistance generation is Kondo scattering and electron-phonon scattering. The former is enhanced due to the decrease in temperature and is characterized by $-\ln T$ dependence of temperature, while the latter weakens. When temperature is lowered to a certain point, Kondo scattering plays the dominating role. Figure 6 presents the electrical resistivity of Eu_2PdSi_3[12] and Tb_2CuGe_3,[34] only showing normal magnetic order instead of Kondo effect. Figure 7 presents electrical resistivity $\rho_{\rm mag}(T)$ of Ce_2CuSi_3,[76] showing a typical Kondo effect. Many R_2TX_3 Kondo compounds have been continuously studied.

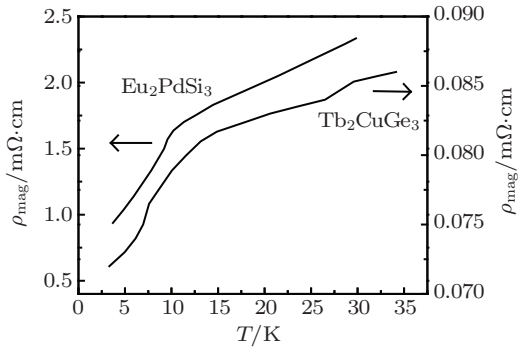


Fig. 6. Temperature dependence of the electrical resistivity for Eu_2PdSi_3[12] and Tb_2CuSi_3.[34]

In 1997, Tien reported the NMAD spin-glass compounds Pr_2CuSi_3[16] and Ce_2CuGe_3,[47] and proposed the existence of Kondo effect. In 1999, Hwang *et al.*[50] reported the similar behavior in Ce_2CuSi_3. In 2009, Kase *et al.*[47] revealed that Ce_2RhSi_3 is an antiferromagnetic Kondo-lattice system with evident anisotropy. In Kondo compounds, one can often find a large negative Curie paramagnetic temperature, which is often used as one of indicators to judge the occurrence of Kondo effect. On the other hand, the external field can also affect the resistance, namely, magnetoresistance (MR). Spin fluctuation and spin-dependent scattering always contribute to the anomaly of MR. The negative sign of MR is consistent with ferromagnetic coupling, while the positive sign is connected with antiferromagnetic coupling. This can be used as another indication of magnetic phase transition. Mallik *et al.*[68] have reported large low-temperature magnetoresistance in Tb_2PdSi_3 and Dy_2PdSi_3. They explained that in zero field there is an antiferromagnetic component undergoing metamagnetic transition with the increase of magnetic field. Majumdar *et al.*[58] reported large negative MR above Curie temperature on polycrystalline Eu_2CuSi_3, and proposed that the observed MR anomaly was merely related to magnetic precursor effect due to 4f magnetism because Cu ions did not carry magnetic moment. Furthermore, the temperature dependence of specific heat also provides the track to magnetic properties. Cao *et al.*[71,78] prepared large single crystals of Eu_2CuSi_3 and examined the properties, where the specific heat implies magnetic fluctuations in the paramagnetic regime and a significant magnetic disorder at $T_{\rm c}$. Actually, the occurrence of the peak in the C–T curve is usually a signature of a magnetic order. For a spin-glass system, no evident singularity is discovered.[62] Nevertheless, in some uncanonical spin-glass systems, the broad bents can still be found, which can be attributed to the formation of magnetic cluster (short-range magnetic order).[65] While in a non-SG system, this bend can be due to Schottky anomalies arising from crystal-field effects. Using the expression $S_{\rm mag} = \int (C_{\rm mag}/T)\,{\rm d}T$, one can obtain the magnetic entropy which further reflects the state of magnetism. For rare-earth ions, if the system reaches the full population of J level, $S = R\ln(2J+1)$,[79] the value of S clarifies the extent of magnetic order and the energy splitting due to CEF. For many ferromagnetic materials near the ferromagnetic transition temperature, the sharp heat capacity at low temperature under zero field broadens with increasing field, which can reflect the ferromagnetic-like ordering of rare-earth ions. This is only one aspect of specific heat responding to magnetic behavior, and other aspects are under research. What attracts attention is the enhancement of γ (specific heat coefficient) in the C/T–T^2 curve. This represents the heavy fermion behavior of R_2TX_3 compounds, which has been found in Ce_2CuSi_3,[38] Pr_2CuSi_3, Kondo effect, and spin glass are respectively responsible for this phenomenon. As a matter of fact, the heavy fermion effect is recognized as the result of the interaction between localized electrons and conduction electrons, where localized electrons are compelled to stay in the dissociative state.

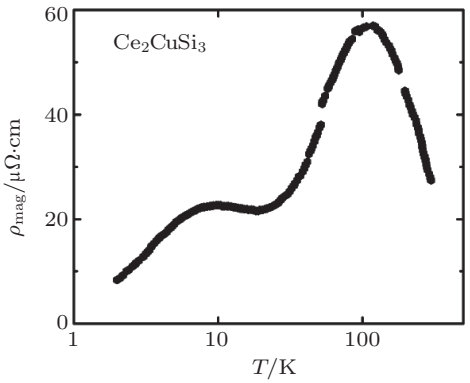


Fig. 7. Temperature dependence of electrical resistivity $\rho_{\rm mag}(T)$ for Ce_2CuSi_3.[76]

8. Conclusion and outlook

The properties of rare-earth ternary compounds R_2TX_3 are abundant, interesting, and fantastic. All the promising findings are strongly correlated with 4f electrons. Different R_2TX_3 compounds present different behaviors in aspects of susceptibility, resistance, specific heat, etc. The magnetism arises from the combined action between RKKY interaction and the CEF effect. However, it is still a tough task to have a clear-cut understanding of the structure and interactional mechanism. This poses a big challenge to improve the theories on the electronic level. For instance, how can we distinguish the spin-glass behavior of amorphous alloys or diluted metallic alloys from that of R_2TX_3 system more accurately and precisely? To solve the problems, it is necessary to establish a more perfect and comprehensive model of structure by establishing phase diagrams,[80] along with the measurements of XRD and electron ray diffraction as well as precise structure computation. Since neutron diffraction is in tight progress, rounding off the current theories on R_2TX_3 can be expected in the near future. Although many synthesized R_2TX_3 compounds have been extensively investigated, some microscopic mechanisms of macroscopic physical properties are far from being perfectly clear. It is absolutely necessary to prepare larger-size single crystals with high quality and get more accurate information on the crystal structures, magnetic structures, and physical properties by neutron diffraction, synchrotron X-ray scattering, and so on. Since the crystal growth techniques are drastically improved,[81–83] large single crystals with high perfection are expected to be grown and more unique phenomena will be revealed in the R_2TX_3 compounds.

References

[1] Chikazumi S 2002 *Physics of Ferromagnetism* (translated by Ge S H) (Lanzhou: Lanzhou University Press) p. 54 (in Chinese)
[2] Dai D S and Qian K M 1998 *Ferromagnetism* (Beijing: Science Press) p. 52 (in Chinese)
[3] Rauchschwalbe U, Lieke W, Bredl C D, Steglich F, Aarts J, Martini K M and Mota A C 1982 *Phys. Rev. Lett.* **49** 1448
[4] Gignoux D, Schmitt D, Zerguine M, Ayache C and Bonjour E 1986 *Phys. Lett. A* **117** 145
[5] Bhattacharjee A K, Coqblin B, Raki M, Forro L, Ayache C and Schmitt D 1989 *J. de Physique* **50** 2781
[6] Ragel F C, du Plessis P D V and Strydom A M 2008 *J. Phys.: Condens. Matter* **20** 055218
[7] Ayache C, Raki M, Salce B, Schmitt D, Bhattacharjee A K and Coqblin B 1988 *J. de Physique* **49** 791
[8] Dalmas de Réotier P, Yaouanc A, Calemczuk R, Huxley A D, Marcenat C, Bonville P, Lejay P, Gubbens P C M and Mulders A M 1997 *Phys. Rev. B* **55** 2737
[9] Grosche F M, Julian S R, Mathur N D and Lonzarich G G 1996 *Physica B* **223** 50
[10] Raymond S, Jaccard D, Wilhelm H and Cerny R 1999 *Solid State Commun.* **112** 617
[11] Demuer A, Holmes A T and Jaccard D 2002 *J. Phys.: Condens. Matter* **14** 529
[12] Mallik R, Sampathkumaran E V, Strecker M, Wortmann G, Paulose P L and Ueda Y 1998 *J. Magn. Magn. Mater.* **185** 135
[13] Rupprecht K, Bielemeier B, Sampathkumaran E V and Wortmann G 2010 *International Conference on the Applications of the Mossbauer Effect*, July 19–24, 2009 Vienna, Austria **217** 012122
[14] Majumdar S, Mallik R, Sampathkumaran E V, Paulose P L and Gopalakrishnan K V 1999 *Phys. Rev. B* **59** 4244
[15] Li D X, Zhao X and Nimori S 2009 *J. Phys.: Condens. Matter* **21** 026006
[16] Tien C, Luo L and Hwang J S 1997 *Phys. Rev. B* **56** 11710
[17] Inosov D S, Evtushinsky D V, Koitzsch A, Zabolotnyy V B, Borisenko S V, Kordyuk A A, Frontzek M, Loewenhaupt M, Löser W, Mazilu I, Bitterlich H, Behr G, Hoffmann J U, Follath R and Büchner B 2009 *Phys. Rev. Lett.* **102** 046401
[18] Chen J W, Guan S Y and Wang C H 2011 *The 2nd International Symposium on Advanced Magnetic Materials and Applications*, July 12–16, 2010 Sendai, Japan **266** 012006
[19] Frontzek M, Kreyssig A, Doerr M, Rotter M, Behr G, Loser W, Mazilu I and Loewenhaupt M 2006 *J. Magn. Magn. Mater.* **301** 398
[20] Szytuła A, Hofmann M, Penc B, Ślaski M, Majumdar S, Sampathkumaran E V and Zygmunt A 1999 *J. Magn. Magn. Mater.* **202** 365
[21] Xu Y K, Frontzek M, MaziluI, Löeser W, Behr G, Buechner B and Liu L 2011 *J. Cryst. Growth* **318** 942
[22] Frontzek M, Kreyssig A, Doerr M, Schneidewind A, Hoffmann J U and Loewenhaupt M 2007 *J. Phys.: Condens. Matter* **19** 145276
[23] Li D X, Nimori S, Shiokawa Y, Haga Y, Yamamoto E and Onuki Y 2003 *Phys. Rev. B* **68** 012413
[24] Kotsandis P A, Yakinthos J K and Gamari-Seale E 1990 *J. Magn. Magn. Mater.* **87** 199
[25] Bażela W, Penc B, Stüesser N, Szytuła A, Wawrzyńska E and Zygmunt A 2004 *Physica B* **350** 167
[26] Bażela W, Wawrzyńska E, Penc B, Stüsser N, Szytuła A and Zygmunt A 2003 *J. Alloys Compd.* **360** 76
[27] Siouris J, Semitelou J P, Yakinthos J K and Schäfer W 2000 *Physica B* **276** 582
[28] Siouris I M, Semitelou I P, Yakinthos J K and Schmitt D 2000 *The 6th European Powder Diffraction Conference*, August 22–25, 1998 Budapest, Hungary **321** 616
[29] Szytuła A, Arulraj A, Baran S, Kaczrowski D, Penc B and Stüsser N 2008 *Solid State Commun.* **147** 61
[30] Siouris I M, Semitelou I P and Yakinthos J K 2000 *J. Alloys Compd.* **297** 26
[31] Siouris I M, Semitelou I P, Yakinthos J K, Arons R R and Schäfer W 2001 *J. Magn. Magn. Mater.* **226** 1128
[32] Semitelou J P, Siouris J, Yakinthos J K, Schäfer W and Schmitt D 1999 *J. Alloys Compd.* **283** 12
[33] Siouris I M, Semitelou I P and Yakinthos J K 2004 *J. Magn. Magn. Mater.* **281** 394
[34] Majumdar S and Sampathkumaran E V 2001 *Solid State Commun.* **117** 645
[35] Raman A 1967 *Naturwiss.* **54** 560
[36] Raman A and Steinfin H 1967 *Inor. Chem.* **6** 1789
[37] Chevalier B, Lejay P, Etourneau J and Hagenmuller P 1984 *Solid State Commun.* **49** 753
[38] Hwang J S, Lin K J and Tien C 1996 *Solid State Commun.* **100** 169
[39] Szytuła A, Hofmann M, Penc B, Ślaski M, Majumdar S, Sampathkumaran E V and Zygmunt A 1999 *J. Magn. Magn. Mater.* **202** 365
[40] Tang F, Frontzek M, Dshemuchadse J, Leisegang T, Zschornak M, Mietrach R, Hoffmann J U, Löeser W, Gemming S, Meyer D C and Loewenhaupt M 2011 *Phys. Rev. B* **84** 104105
[41] Gschneidner K A Jr and Eyring L (1978–1998) *Handbook on the Physics and Chemistry of Rare Earths* (Holland: Amsterdam)
[42] Hoffmann R D and Pöttgen R 2001 *Z. Kristallogr.* **216** 127
[43] Pöttgen R and Kaczorowski D 1993 *J. Alloys Compd.* **201** 157
[44] Li D X, Nimori S, Yamamura T and Shiokawa Y 2008 *J. Appl. Phys.* **103** 07B715
[45] Tran V H 1996 *J. Phys.: Condens. Matter* **8** 6267
[46] Li D X, Dönni A, Kimura Y, Shiokawa Y, Homma Y, Haga Y, Yamamoto E, Honma T and Onuki Y 1999 *J. Phys.: Condens. Matter* **11** 8263
[47] Tien C, Feng C H, Wur C S and Lu J J 2000 *Phys. Rev. B* **61** 12151
[48] Peter S C, Sarkar S and Kanatzidis M G 2012 *Inorg. Chem.* **51** 10793
[49] Yamamura T, Li D X and Shiokawa Y 2003 *Physica B* **329** 559
[50] Kase N, Muranaka T and Akimitsu J 2009 *J. Magn. Magn. Mater.* **321** 3380
[51] Chevalier B, Lejay P, Etourneau J and Hagenmuller P 1984 *Solid State Commun.* **49** 753

[52] Gladyshevskii R E, Cenzual K and Parthé E 1992 *J. Alloys Compd.* **189** 221

[53] Szlawska M and Kaczorowski D 2011 *Phys. Rev. B* **84** 094430

[54] Gordon R A, Warren C J, Alexander M G, Disalvo FJ and Pöttgen R 1997 *J. Alloys Compd.* **248** 24

[55] Yubuta K, Yamamura T and Shiokawa Y 2006 *J. Phys.: Condens. Matter* **18** 6109

[56] Rojas D P, Rodríguez Fernández J, Espeso J I, Gómez Sal J C, da Silva L M, Gandra F G, dos Santos A O and Medina A N 2010 *J. Magn. Magn. Mater.* **322** 3192

[57] Nimori S and Li D X 2006 *J. Phys. Soc. Jpn.* **75** 195

[58] Majumdar S, Mallik R, Sampathkumaran E V, Rupprecht K and Wortmann G 1999 *Phys. Rev. B* **60** 6770

[59] Li D X, Nimori S, Shiokawa Y, Haga Y, Yamamoto E and Onuki Y 2001 *Solid State Commun.* **120** 227

[60] Siouris I M, Semitelou I P, Yakinthos J K, Schäfer W and Arons R R 2001 *J. Alloys Compd.* **314** 1

[61] Yamamura T, Li D, Yubuta K and Shiokawa Y 2004 *J. Alloys Compd.* **374** 226

[62] Li D X, Shiokawa Y, Homma Y, Uesawa A, Dönni A, Suzuki T, Haga Y, Yamamoto E, Honma T and Onuki Y 1998 *Phys. Rev. B* **57** 7434

[63] Yamamura T, Li D X, Yubuta K and Shiokawa Y 2006 *J. Alloys Compd.* **408** 1324

[64] Li D X, Nimori S, Shiokawa Y, Tobo A, Onodera H, Haga Y, Yamamoto E and Onuki Y 2001 *Appl. Phys. Lett.* **79** 4183

[65] Li D X, Yamamura T, Yubuta K, Nimori S, Haga Y and Shikama T 2011 *International Conference on Frustration in Condensed Matter*, January 11–14, 2011 Sendai, Japan **320** 012041

[66] Frontzek M, Kreyssig A, Doerr M, Hoffman J U, Hohlwein D, Bitterlich H, Behr G and Loewenhaupt M 2004 *Physica B* **350** 187

[67] Huo D X, Sakurai J, Kuwai T, Isikawa Y and Lu Q F 2001 *Phys. Rev. B* **64** 224405

[68] Mallik R, Sampathkumaran E V and Paulose P L 1998 *Solid State Commun.* **106** 169

[69] Li D X, Nimori S, Yamamura T, Yubuta K, Shirazaki K and Zhao X 2009 *J. Alloys Compd.* **488** 558

[70] Yamamura T, Li D X, Yubuta K and Shiokawa Y 2006 *J. Alloys Compd.* **408** 1324

[71] Nishioka T, Tabata Y, Taniguchi T and Miyako Y 2000 *J. Phys. Soc. Jpn.* **69** 1012

[72] Siouris I M, Kremer R K and Hoelzel M 2011 *J. Magn. Magn. Mater.* **323** 2903

[73] Siouris I M 2007 *J. Magn. Magn. Mater.* **309** 222

[74] Szlawska M, Pikul A and Kaczorowski D 2007 *Mater. Sci.* **25** 1267

[75] Gschneidner K A and Pecharsky V K 1996 *Physica B* **223** 131

[76] Nakamoto G, Shibai Y, Kurisu M and Andoh Y 2000 *Physica B* **281** 76

[77] Cao C D, Klingeler R, Vinzelberg H, Leps N, Löeser W, Behr G, Muranyi F, Kataev V and Buechner B 2010 *Phys. Rev. B* **82** 134446

[78] Cao C D, Löser W, Behr G, Klingeler R, Leps N, Vinzelberg H and Büchner B 2011 *J. Cryst. Growth* **318** 1009

[79] Rojas D P, Fernández J R, Espeso J I and Gómez Sal J C 2010 *J. Magn. Magn. Mater.* **322** 3192

[80] Behr G, Löser W, Graw G, Bitterlich H, Fink J and Schultz 2000 *Cryst. Res. Technol.* **35** 461

[81] Luedge A, Riemann H, Wuenscher M, Behr G, Loeser W, Muiznieks A and Croell A 2010 *Floating Zone Crystal Growth in Crystal Growth Processes Based on Capilarity*: *Czochralski, Floating Zone, Shaping and Crucible Techniques* (Chichester: John Wiley and Sons) pp. 203–275

[82] Cao C D, Deppe M, Behr G, Löser W, Wizent N and Büchner B 2011 *Crystal Growth Design* **11** 431

[83] Cao C D, Klingeler R, Leps N, Vinzelberg H, Kataev V, Muranyi F, Tristan N, Teresiak A, Zhou S Q, Löser W, Behr G and Büchner B 2008 *Phys. Rev. B* **78** 064409